AIAA JOURNAL
Vol. 38, No. 2, February 2000

Iterative Space-Marching Method for Compressible Sub-, Trans-, and Supersonic Flows

N. K. Yamaleev*
Institute of Mathematics, 450000, Ufa, Russia
and
J. Ballmann†
Technical University of Aachen, 52062 Aachen, Germany

A new iterative fully coupled implicit space-marching method is proposed for solving the two-dimensional steady Euler equations for compressible flows at Mach numbers ranging from subsonic to supersonic. A special treatment of the streamwise pressure gradient component permits us to calculate both supersonic flow regions, where the Euler equations are hyperbolic, and subsonic regions, where the equations reveal elliptic properties. To take into account the elliptic effects of subsonic and transonic flows, space-marching sweeps are carried out iteratively. A new parabolic pressure correction procedure is developed to accelerate the convergence rate. This procedure can be applied for subsonic and transonic regimes and is consistent with the characteristic analysis of the Euler equations. At each marching station, a Newton iterative technique is used to solve the nonlinear system of equations in a fully coupled manner. To resolve strong shocks and contact discontinuities as well as smooth flowfields with high accuracy, implicit symmetric second-order total variation diminishing and upwind second-order Richardson schemes are employed to approximate the transverse and streamwise derivatives, respectively. The method is tested on the problem of the flow in a duct with a circular arc bump for different Mach number regimes. Numerical calculations show that the method is accurate, is robust, and can efficiently be applied for calculating subsonic, transonic, and supersonic flows without streamwise separation.

Nomenclature

a	= eigenvalues of $\partial\tilde{\boldsymbol{F}}/\partial\boldsymbol{U}$
c	= speed of sound
$\boldsymbol{E}, \boldsymbol{F}$	= inviscid flux vectors in Cartesian coordinates
$\tilde{\boldsymbol{E}}, \tilde{\boldsymbol{F}}$	= inviscid flux vectors in curvilinear coordinates
e_t	= total energy per unit volume
$\boldsymbol{H}$	= the corrected numerical flux vector consistent with $\tilde{\boldsymbol{F}}$
H	= total enthalpy
J	= Jacobian of the coordinate mapping
L	= reference length
M_ξ	= local streamwise Mach number
$\boldsymbol{n}$	= vector normal to the wall
p	= static pressure
$\tilde{p}$	= pressure field calculated from the current global iteration
Q	= limiter
R	= matrix of the right eigenvectors of $\partial\tilde{\boldsymbol{F}}/\partial\boldsymbol{U}$
$r^{\pm}$	= ratios of neighboring gradients of the characteristic variables
$\boldsymbol{U}$	= vector of conservation variables
u, v	= Cartesian velocity components
$\boldsymbol{V}$	= velocity vector
x, y	= Cartesian coordinates
α	= difference of the characteristic variables in η direction
γ	= ratio of specific heats
$\Delta\xi, \Delta\eta$	= grid step sizes in ξ and η
$\Delta^k f$	= $f^{k+1} - f^k$
δ	= small positive number
$\epsilon_{i,j}, \delta_{i,j}$	= pressure corrections
μ	= diffusion factor for the pressure correction procedure
ξ, η	= general curvilinear coordinates
$\xi_x, \xi_y, \eta_x, \eta_y$	= metric coefficients
ρ	= gas density
σ	= safety factor
τ	= relaxation parameter, $0 \le \tau \le 1$
ω	= parameter for the pressure gradient splitting, $0 \le \omega \le 1$

Subscript

$-\infty$	= far upstream values

Superscripts

in	= inflow values
k	= kth local Newton iteration
l	= lth vector component
n	= nth global iteration
out	= outflow values
$'$	= dimensional quantities

I. Introduction

A NUMBER of space-marching methods have been developed for calculating both incompressible and compressible flows. These methods can be divided into two parts: 1) methods for solving the incompressible form of the reduced or full Navier–Stokes equations[1–4] and 2) methods for solving the compressible form of the reduced Navier–Stokes equations for super- or hypersonic flows.[5–11]

The first class of methods have been elaborated for incompressible or low Mach number flows. To resolve the elliptic effects of essentially subsonic or incompressible flows, multiple space-marching sweeps are carried out with respect to the streamwise pressure gradient component that is approximated by forward differences and treated as a source term in the whole computational domain. This treatment of the pressure gradient term permits information to be propagated in the upstream direction that corresponds to the elliptic nature of incompressible or quasi-incompressible flows. This approach has successfully been applied to calculate incompressible viscous flows with strong streamwise separation.[1–4] However, these methods cannot be directly used for calculating transonic and

Received 25 April 1998; revision received 14 June 1999; accepted for publication 17 June 1999.

*Senior Research Scientist, Department of Computational Mathematics.
†Professor, Lehr- und Forschungsgebiet für Mechanik. Member AIAA.

supersonic flow regions, where the steady Euler equations reveal hyperbolic–elliptic and hyperbolic properties, respectively.

The second class of methods can be employed for predicting supersonic viscous flows with a thin subsonic layer[5–10] or flows with local subsonic regions (such as a blunt-body nose region) embedded into the main supersonic stream.[11] The principal difference between methods belonging to the second class is the treatment of the streamwise pressure gradient component in subsonic flowfields. In the single sweep procedure offered by Vigneron et al.[7] for the parabolized Navier–Stokes equations describing weakly interacting flows, the streamwise pressure gradient term is neglected in subsonic regions. For that reason, this approach may result in either considerable errors for essentially transonic flows or completely wrong solutions for fully subsonic flows. Another procedure has been developed in Ref. 9. In this method, the pressure gradient term in a thin subsonic sublayer near the body surface is estimated at the first grid point where the flow is supersonic. The sublayer approximation is based on the asymptotic boundary-layer theory appropriate for high-Reynolds-number flows along walls with a small curvature. However, this technique cannot be used for simulating essentially transonic or completely subsonic flows, where the sublayer approximation is not valid. The most general approach is to retain the pressure gradient term in subsonic regions and approximate it by forward differences,[10,11] so that the downstream pressure is taken from the previous iteration and treated as a source term that corresponds to the elliptic properties of subsonic flows. This approximation combined with the streamwise pressure gradient splitting[7] is used in the present study and enables one to calculate compressible sub-, trans-, and supersonic flows.

At each marching station, the nonlinear system of equations resulted from the discretization procedure has to be solved. There are three basic approaches to solve this problem: 1) a coupled noniterative method,[7] 2) a coupled quasi-time-dependent method,[8] and 3) an uncoupled or semicoupled iterative method.[9–11] The main disadvantage of the first one is an error introduced by the approximate factorization of the nonlinear equations. It may result that some important physical phenomena can be distorted or even be lost due to the linearization. The principal drawback of the second approach is that the convergence rate of the iteration process is rather slow because of the presence of the fictitious time-dependent term in the governing equations. One of the shortcomings of the third technique is its sensitivity to changes of initial data or geometry because the velocity components and pressure are computed from different algorithms in a decoupled manner. To overcome these problems, a fully coupled iterative method is proposed. The method is based on a Newton iterative approach applied to the system of nonlinear equations rather than to each equation separately. It reduces the factorization error to zero and permits us to solve the nonlinear set of equations in a fully coupled manner.

It is well known that the convergence rate of a usual multiple space-marching procedure is slow if subsonic regions are large. Several strategies have been developed to accelerate the convergence. One of the widely used approaches is the semi-implicit pressure-correction method of Patankar and Spalding[12] based on the solution of a Poisson equation for pressure or its generalizations.[13–15] Because this procedure in its standard form leads to an elliptic equation for pressure or pressure correction, it is not consistent with hyperbolic properties of transonic and supersonic flows. Furthermore, this approach is very time consuming because the elliptic equation for pressure must be solved at each global iteration. Another pressure correction procedure has been proposed by Davis et al.[16] The main idea of the method is to introduce a fictitious time-dependent term into the streamwise momentum equation. Despite the fact that the solution of the hyperbolic equation is short compared with computational efforts required for one space-marching sweep, there are two main drawbacks of that approach. First, the pressure-correction procedure may lead to numerical instabilities caused by the lack of diffusive mechanisms in the transverse direction resulting in considerable skewing of the transverse pressure profiles. Second, the introduction of the time-dependent term into the global iteration procedure essentially decreases the effectiveness of the algorithm especially for transonic flows. To combine the diffusive effects of the Poisson equation with the signal propagation properties of the hyperbolic algorithm, a parabolic pressure-correction procedure elaborated in Ref. 4 for incompressible flows is generalized in the present paper to calculate compressible flows at all speeds. In contrast to the procedure developed in Ref. 4, the present technique is consistent with the characteristics in regions where the Euler equations are hyperbolic, and consequently, it can be employed for subsonic, transonic, and supersonic flows.

An implicit space-marching method based on the global pressure relaxation procedure has been elaborated in Ref. 17 to solve the steady Euler equations for subsonic, transonic, and supersonic flows. In this approach the equations are solved in a decoupled manner by using two-point backward differences for the streamwise derivatives and central and trapezoidal rule approximations for the transverse derivatives that makes the method very sensitive to the grid spacing. Therefore, a very fine grid has to be used to provide stability of the space-marching sweep and to resolve shock waves with sufficient accuracy. In turn, it considerably decelerates the convergence rate because no pressure correction has been made and information is propagated one station upstream per iteration.

The main purpose of the present work is to develop an iterative fully coupled space-marching method applicable at all Mach numbers. This high-resolution method using the parabolic pressure-correction procedure can efficiently be employed to calculate both smooth subsonic flows and transonic or supersonic flows with strong shocks, contact discontinuities, and rarefaction waves and their interaction with high accuracy by using a moderate number of grid nodes.

II. Governing Equations and Boundary Conditions

A. Governing Equations

The nondimensionalized two-dimensional steady Euler equations in Cartesian coordinates can be written in the strong conservation law form as

$$\frac{\partial \boldsymbol{E}}{\partial x} + \frac{\partial \boldsymbol{F}}{\partial y} = 0 \tag{1}$$

$$\boldsymbol{E} = \begin{bmatrix} \rho u \\ \rho u^2 + p \\ \rho v u \\ u(e_t + p) \end{bmatrix}, \qquad \boldsymbol{F} = \begin{bmatrix} \rho v \\ \rho v u \\ \rho v^2 + p \\ v(e_t + p) \end{bmatrix}, \qquad \boldsymbol{U} = \begin{bmatrix} \rho \\ \rho u \\ \rho v \\ e_t \end{bmatrix}$$

The system of equations (1) is closed using the equation of state for a perfect gas flow, which is given by

$$e_t = p/(\gamma - 1) + (\rho/2)(u^2 + v^2)$$

The nondimensionalized variables in Eq. (1) are defined in the following manner:

$$x = x'/L', \qquad y = y'/L', \qquad u = u'/V'_{-\infty}, \qquad v = v'/V'_{-\infty}$$

$$\rho = \rho'/\rho'_{-\infty}, \qquad p = p'/\rho'_{-\infty} V'^2_{-\infty}, \qquad e_t = e'_t/\rho'_{-\infty} V'^2_{-\infty}$$

To simplify the treatment of arbitrary geometries, a general coordinate transformation

$$\xi = \xi(x, y), \qquad \eta = \eta(x, y) \tag{2}$$

is used to map a physical domain with curvilinear boundaries onto a unit square. As a result of this transformation, the Euler equations can be represented in the strong conservation law form as follows:

$$\frac{\partial \tilde{\boldsymbol{E}}}{\partial \xi} + \frac{\partial \tilde{\boldsymbol{F}}}{\partial \eta} = 0$$

$$\tilde{\boldsymbol{E}} = 1/J(\xi_x \boldsymbol{E} + \xi_y \boldsymbol{F}), \qquad \tilde{\boldsymbol{F}} = 1/J(\eta_x \boldsymbol{E} + \eta_y \boldsymbol{F}) \tag{3}$$

where the Jacobian of the mapping is given by

$$J = \frac{\partial(\xi, \eta)}{\partial(x, y)} = \xi_x \eta_y - \xi_y \eta_x = \frac{1}{x_\xi y_\eta - x_\eta y_\xi}$$

B. Boundary Conditions

To close the governing equations (3), boundary conditions should be specified. In the present analysis only channel flows are considered. Therefore, without loss of generality it is assumed that the physical domain is bounded by four boundaries. The left and right boundaries correspond to the inflow and outflow, accordingly, and the upper and lower boundaries are the duct walls.

Furthermore, we assume that the inflow and outflow boundaries are far enough upstream and downstream, respectively, so that the flow is uniform there. Hence, the locally quasi-one-dimensional approach based on the theory of characteristics can be applied to impose the appropriate boundary conditions at these boundaries.

If the inflow is supersonic, all flow quantities are prescribed at the upstream boundary:

$$\boldsymbol{U}|_{\xi=0} = \boldsymbol{U}_0(\eta) \tag{4}$$

If the inflow is subsonic, the boundary conditions corresponding to the characteristics C^+ and C^0 coming from outside of the physical domain are specified by the Riemann invariant along C^+ and the value of the constant in the isentropic pressure density relation

$$v + \left.\frac{2c}{\gamma-1}\right|_{\xi=0} = v^{\text{in}} + \frac{2c^{\text{in}}}{\gamma-1}$$

$$\left.\frac{p}{\rho^\gamma}\right|_{\xi=0} = \frac{p^{\text{in}}}{(\rho^{\text{in}})^\gamma}, \qquad \left.\frac{v}{u}\right|_{\xi=0} = 0 \tag{5}$$

At a supersonic downstream boundary, no boundary conditions are prescribed. As follows from the characteristic analysis, at a subsonic outlet boundary a boundary condition for the static pressure should be imposed. In the present work, this condition is replaced by the Riemann invariant that corresponds to the characteristic C^- coming from outside of the physical domain to the outflow boundary:

$$v - [2c/(\gamma-1)]|_{\xi=1} = v^{\text{out}} - [2c^{\text{out}}/(\gamma-1)] \tag{6}$$

At the solid impermeable duct walls, the contact conditions for the normal velocity component are used:

$$\boldsymbol{V}\cdot\boldsymbol{n}|_{\eta=0} = \boldsymbol{V}\cdot\boldsymbol{n}|_{\eta=1} = 0 \tag{7}$$

III. Iterative Space-Marching Method

For subsonic flow regions the system of partial differential equations (3) is elliptic with respect to the spatial coordinate ξ, which is assumed to be close to or coinciding with the main flow direction. As it follows from the theoretical analysis, the initial-value problem is ill posed for an elliptic system of equations. Hence, it is impossible to solve the Euler equations for stationary subsonic flows by using a noniterative space-marching technique.

However, if the streamwise pressure gradient component is specified and can, therefore, be treated as a source term, the Euler equations altered this way are hyperbolic at all flow speeds.[16] Consequently, the modified Euler equations can be solved for one space-marching sweep through the computational domain. A more general approach has been proposed by Vigneron et al.[7] The basic idea of the method is to split the streamwise pressure gradient term as follows:

$$\frac{\partial p}{\partial \xi} = \omega\left(\frac{\partial \tilde{p}}{\partial \xi}\right) + (1-\omega)\left(\frac{\partial p}{\partial \xi}\right)^{n-1} \tag{8}$$

where the first term on the right-hand side of Eq. (8) is calculated implicitly during the current marching sweep and the second term is evaluated from the previous iteration and treated as a source term.

After the splitting, the transformed Euler equations become hyperbolic and the Cauchy problem is well posed as an initial value problem in the spatial coordinate ξ if

$$0 \le \omega \le \Omega(u, v, c) = \frac{\gamma M_\xi^2}{1 + (\gamma-1)M_\xi^2}, \qquad \xi_x u + \xi_y v \ge 0 \tag{9}$$

These conditions can be incorporated into the space-marching algorithm as follows:

$$\omega = \min[1, \sigma\Omega(u, v, c)] \tag{10}$$

where σ is a safety factor that was set equal to 0.8 in the numerical calculations.

To account for the elliptic nature of subsonic and transonic flows and to find the solution of the original Euler equations, the space-marching sweeps should be repeated iteratively. These so-called global iterations must provide the propagation of information in the upstream direction in subsonic regions.

Note that it is impossible to use backward differences for approximating the second term in Eq. (8), as was suggested in Ref. 7, because it leads to divergence or growing exponential solutions. This kind of divergent solution can easily be explained by an unsuccessful attempt to treat the elliptic system of equations as an initial-value problem.

The most appropriate approach for handling the pressure gradient term $(1-\omega)\partial p/\partial \xi$ is to approximate it by a forward difference, so that the unknown downstream pressure is lagged and taken from the previous global iteration. In other words, the term transmitting the information about the downstream flow conditions is treated as a source term that provides the numerical stability in the space-marching sweep and that corresponds to the elliptic nature of the Euler equations for subsonic flows.

Note that a widely used approximation of the p_ξ term

$$\left(\frac{\partial p}{\partial \xi}\right)_i = \omega_i \frac{p_i - p_{i-1}}{\Delta\xi} + (1-\omega_i)\frac{p_{i+1} - p_i}{\Delta\xi} \tag{11}$$

is nonconservative. A simple analysis shows that this approximation is conservative if $\omega_i = 0.5(\omega_{i-1} + \omega_{i+1})$. It means that the approximation Eq. (11) reveals conservative properties only for smooth flows, whereas it is nonconservative at shocks and contact discontinuities, where the conservativeness is particularly important.

On the other hand, a strongly conservative approximation of the pressure gradient term, that is,

$$\left(\frac{\partial p}{\partial \xi}\right)_i = \frac{\omega_i p_i - \omega_{i-1} p_{i-1}}{\Delta\xi} + \frac{(1-\omega_{i+1})p_{i+1} - (1-\omega_i)p_i}{\Delta\xi} \tag{12}$$

is much too diffusive. This can easily be shown by representing Eq. (12) in semidiscrete form:

$$\left(\frac{\partial p}{\partial \xi}\right)_i = \frac{p_{i+1} - p_i}{\Delta\xi} - \frac{\omega_{i-1}p_{i-1} - 2\omega_i p_i + \omega_{i+1}p_{i+1}}{\Delta\xi}$$

$$= \frac{p_{i+1} - p_i}{\Delta\xi} - \Delta\xi\omega_i\left(\frac{\partial^2 p}{\partial \xi^2}\right)_i - \Delta\xi p_i\left(\frac{\partial^2 \omega}{\partial \xi^2}\right)_i \tag{13}$$

Equation (13) may be interpreted as follows. The second term on the right-hand side provides the switching from backward to forward differences, corresponding to the hyperbolic–elliptic type of the Euler equations. The last term is additional artificial dissipation achieving its maximum values at shocks and rarefaction waves, where the Mach number rapidly changes.

In the present method, Eq. (8) is approximated by

$$\left(\frac{\partial p}{\partial \xi}\right)_i = \omega_i \frac{p_i - p_{i-1}}{\Delta\xi} + (1-\omega_{i+1})\frac{p_{i+1} - p_i}{\Delta\xi} \tag{14}$$

Such an evaluation of Eq. (8) originally proposed in Ref. 17 provides conservation properties across flow discontinuities, which are very important for calculating transonic and supersonic flows. To show that the preceding approximation of the term $\partial p/\partial \xi$ is strongly conservative, we rewrite Eq. (14) as follows:

$$\left(\frac{\partial p}{\partial \xi}\right)_i = \frac{\omega_{i+1}p_i + (1-\omega_{i+1})p_{i+1} - [\omega_i p_{i-1} + (1-\omega_i)p_i]}{\Delta\xi} \tag{15}$$

By defining a new pressure value p^c at the $i+\frac{1}{2}$ point as

$$p^c_{i+\frac{1}{2}} = \omega_{i+1} p_i + (1-\omega_{i+1}) p_{i+1}$$

Eq. (14) can be represented in strong conservation form

$$\left(\frac{\partial p}{\partial \xi}\right)_i = \frac{p^c_{i+\frac{1}{2}} - p^c_{i-\frac{1}{2}}}{\Delta \xi} \tag{16}$$

Consequently, Eq. (14) leads to the conservative approximation of the streamwise pressure gradient term.

To apply this technique, the flux vector $\tilde{\boldsymbol{E}}$ is split into two parts,

$$\tilde{\boldsymbol{E}} = \tilde{\boldsymbol{E}}^* + \boldsymbol{P}^*, \qquad \tilde{\boldsymbol{E}}^* = (1/J)(\xi_x \boldsymbol{E}^* + \xi_y \boldsymbol{F}^*)$$

$$\boldsymbol{P}^* = [0, (\xi_x/J)p, (\xi_y/J)p, 0]^T \tag{17}$$

By substitution of Eqs. (8) and (17) in Eq. (3), the final form of the governing equations becomes

$$\frac{\partial \tilde{\boldsymbol{E}}^*}{\partial \xi} + \frac{\partial \tilde{\boldsymbol{F}}}{\partial \eta} = -\omega\left(\frac{\partial \boldsymbol{P}^*}{\partial \xi}\right) - (1-\omega)\left(\frac{\partial \boldsymbol{P}^*}{\partial \xi}\right)^{n-1} \tag{18}$$

where the first term on the right-hand side is calculated implicitly and the second term is taken from the previous global iteration and treated as a known source term during the current global iteration.

We want to emphasize that the splitting just presented differs from the Vigneron et al.[7] flux vector splitting where the term ωp is included into the flux vector $\tilde{\boldsymbol{E}}^*$. The parameter ω is functionally dependent on M_ξ, and its derivative is discontinuous at $M_\xi = 1$. Furthermore, ω is a discontinuous function at shocks and contact discontinuities. Therefore, the Vigneron et al. splitting, which implicitly contains the term $p\partial\omega/\partial\xi$, may exhibit nonphysical oscillations near the sonic line and at strong discontinuities of the solution. The splitting represented by Eqs. (17) and (18) enables one to eliminate the term ω_ξ from the governing equations. That ensures nonoscillatory behavior of the numerical solution both in the vicinity of the sonic line and near strong gradients of the streamwise Mach number.

The solution of the original Euler equations [Eq. (3)] is found by repeated space-marching sweeps through the computational domain. However, this approach may require a large number of iterations because a signal is propagated only one station upstream for each global iteration. To accelerate the convergence of the iteration process, a parabolic pressure-correction procedure is proposed. This method is described in Sec. V.

IV. Numerical Method

A. Fully Coupled Iterative Method

As already mentioned, for subsonic, transonic, and supersonic nonseparated flows, the modified Euler equations [Eq. (18)] are hyperbolic in the marching coordinate ξ. Taking into account the analysis described in the preceding section, the derivatives in the streamwise direction ξ in Eq. (18) are evaluated by implicit first-order backward differences for $\partial\tilde{\boldsymbol{E}}^*/\partial\xi$ and $\omega\partial\boldsymbol{P}^*/\partial\xi$ terms and by forward differences for the pressure gradient term $(1-\omega)\partial\boldsymbol{P}^*/\partial\xi$. Without specifying the discretization of the derivatives in the transverse direction η, one can write

$$\frac{\tilde{\boldsymbol{E}}^*_i - \tilde{\boldsymbol{E}}^*_{i-1}}{\Delta\xi} + \left(\frac{\partial \tilde{\boldsymbol{F}}}{\partial \eta}\right)_i = -\omega_i \frac{\boldsymbol{P}^*_i - \boldsymbol{P}^*_{i-1}}{\Delta\xi} - (1-\omega_{i+1})\frac{\boldsymbol{P}^{*\,n-1}_{i+1} - \boldsymbol{P}^*_i}{\Delta\xi} \tag{19}$$

One of the algorithms employed frequently for solving Eq. (19) is the coupled noniterative method originally proposed by Vigneron et al.[7] The main idea of the method is to apply the implicit approximate factorization algorithm of Ref. 18 to the governing equations, so that the system of nonlinear equations (19) is linearized in the neighborhood of the section $\xi = \xi_{i-1}$. However, the solution of the linearized equations only approximates the solution of Eq. (19). The discrepancy between these two solutions can be perceptible when the streamwise gradient of the solution is sufficiently high or when the integration step size $\Delta\xi$ is large. On the other hand, some important physical properties of the nonlinear equations may be lost because of the linearization.

To find the solution of the original nonlinear equations (19), a fully coupled iterative procedure is proposed. Instead of the linearization of the nonlinear equations (19) with respect to the previous marching station $\xi = \xi_{i-1}$ as in Ref. 7, we apply the Newton iterative method to the entire nonlinear system of equations Eq. (19), rather than to each equation separately as it was done in Refs. 6 and 9–11. That results in the following linear system of equations written in the delta form:

$$\left[\frac{1}{\Delta\xi}\left(\frac{\partial \tilde{\boldsymbol{E}}^*}{\partial \boldsymbol{U}}\right)^k_i + \frac{\partial}{\partial\eta}\left(\frac{\partial \tilde{\boldsymbol{F}}}{\partial \boldsymbol{U}}\right)^k_i - \frac{1-\omega_i-\omega_{i+1}}{\Delta\xi}\left(\frac{\partial \boldsymbol{P}^*}{\partial \boldsymbol{U}}\right)^k_i\right]\Delta^k \boldsymbol{U}_i$$

$$= -\left\{\frac{\tilde{\boldsymbol{E}}^{*k}_i - \tilde{\boldsymbol{E}}^*_{i-1}}{\Delta\xi} + \left(\frac{\partial \tilde{\boldsymbol{F}}}{\partial\eta}\right)^k_i + \omega_i \frac{\boldsymbol{P}^{*k}_i - \boldsymbol{P}^{*k}_{i-1}}{\Delta\xi} + (1-\omega_{i+1})\frac{\boldsymbol{P}^{*n-1}_{i+1} - \boldsymbol{P}^{*k}_i}{\Delta\xi}\right\} \tag{20}$$

The main difference between Eq. (20) and the factorization algorithm is that at every marching station ξ_i the left-hand side of Eq. (20) becomes zero upon convergence. This implies that Eq. (19), which corresponds to the right-hand side of Eq. (20), is satisfied at each marching station. It is important to emphasize that the iterative scheme [Eq. (20)] is converted to the noniterative linearized scheme[7] if the initial guess required for the Newton algorithm is taken to be equal to the solution found at the previous marching station ξ_{i-1} and only one iteration is performed. Also, the solution of Eq. (20) enables one to estimate the error introduced by the approximate factorization. In the neighborhood of strong gradients in the flowfield, as well as near wall slope discontinuities, the underrelaxation of the predicted solution was used. Numerical calculations show that to reduce the residual to the desired convergence level ($\epsilon = 10^{-5}$) only two to six Newton iterations are required.

The main disadvantage of the iterative approach is the additional computational effort due to the iterations. This difficulty can be partly overcome by using larger grid spacing in the marching direction than for the noniterative algorithm. This is possible because the fully coupled iterative method is more stable and more accurate than its noniterative counterpart. The linearization introduces some additional errors that makes the numerical algorithm more unstable, whereas the iterative scheme reduces the factorization error to zero at every marching station, which improves both stability and accuracy.

B. Finite Difference Scheme

A very broad class of approximations can be applied to evaluate the derivatives in the transverse direction η. To capture flowfields with strong shock waves and contact discontinuities, a difference scheme should have the following properties: 1) conservativeness, 2) high-order accuracy, 3) quasi monotonicity.

The symmetric total variation diminishing (TVD) scheme developed by Yee[19] meets all three of the preceding demands. The conservative nature and second-order accuracy of this TVD scheme ensure the resolution of flow discontinuities without spurious oscillations and with only small numerical dissipation resulting in the smearing of shocks and contact discontinuities over 1–3 grid cells.

The conservative approximation of the derivative $\tilde{\boldsymbol{F}}_\eta$ is given by

$$\left(\frac{\partial \tilde{\boldsymbol{F}}}{\partial \eta}\right)_j = \frac{\boldsymbol{H}_{j+\frac{1}{2}} - \boldsymbol{H}_{j-\frac{1}{2}}}{\Delta\eta} \tag{21}$$

The corrected numerical flux for the second-order symmetric TVD scheme[19] is

$$\boldsymbol{H}_{j+\frac{1}{2}} = \tfrac{1}{2}\left[\tilde{\boldsymbol{F}}_j + \tilde{\boldsymbol{F}}_{j+1} - R_{j+\frac{1}{2}}\Phi_{j+\frac{1}{2}}\right] \tag{22}$$

where the components of the vector $\Phi_{j+1/2}$ in Eq. (22) are defined by

$$\phi^l_{j+\frac{1}{2}} = \left[\frac{\Delta\xi}{\Delta\eta}\left(a^l_{j+\frac{1}{2}}\right)^2 Q^l_{j+\frac{1}{2}} + \psi\left(a^l_{j+\frac{1}{2}}\right)\left(1 - Q^l_{j+\frac{1}{2}}\right)\right]\alpha^l_{j+\frac{1}{2}} \tag{23}$$

with

$$\alpha_{j+\frac{1}{2}} = \frac{R^{-1}_{j+\frac{1}{2}}(\boldsymbol{U}_{j+1} - \boldsymbol{U}_j)}{0.5(J_{j+1} + J_j)}, \qquad \psi(z) = \begin{cases} |z|, & |z| \geq \delta \\ \dfrac{z^2 + \delta^2}{2\delta}, & |z| < \delta \end{cases} \tag{24}$$

The TVD correction of the numerical flux vector $\tilde{\boldsymbol{F}}_{j+1/2}$ in Eq. (22) results in the scheme approximating the transverse derivatives with second-order accuracy in regions where the solution is smooth and with first-order accuracy near local extrema and discontinuities of the numerical solution.

The limiter $Q^l_{j+1/2}$ in Eq. (23) determines the principal dissipative properties of the TVD scheme and is responsible for the feedback mechanism that enables one to control the numerical dissipation in accordance with the ratio of the neighboring gradients of the characteristic quantities.

The limiter $Q^l_{j+1/2}$ used in this paper is calculated as follows:

$$Q^l_{j+\frac{1}{2}} = \max\{0, \min(2r^-, 1) + \min(2r^+, 1) - 1\} \tag{25}$$

where the ratios of the neighboring gradients of the characteristic variables are given by

$$r^- = \frac{\alpha^l_{j-\frac{1}{2}}}{\alpha^l_{j+\frac{1}{2}}}, \qquad r^+ = \frac{\alpha^l_{j+\frac{3}{2}}}{\alpha^l_{j+\frac{1}{2}}}$$

Numerical calculations of the Riemann problem have shown that the limiter equation (25) produces steep shock wave fronts and does not lead to the production of spurious oscillations in the vicinity of strong gradients of the solution.

The TVD scheme [Eqs. (20–25)] is defined with a five-point grid bandwidth including the points from $j-2$ to $j+2$ in the coordinate η. Nevertheless, the linearized system of equations (20) has a block-tridiagonal matrix instead of a block-pentadiagonal matrix. In fact, the five-point grid bandwidth of the present TVD scheme is determined by the limiter $Q^l_{j\pm1/2}$, which depends on the solution found at the previous Newton iteration. For that reason, the limiter is a known function at the current Newton iteration. Hence, at the marching level ξ_i, the bandwidth of the scheme [Eq. (20–25)] includes only three grid points that result in a block-tridiagonal matrix on the left-hand side of Eq. (20). This matrix can be reversed by the standard block-elimination procedure.

The finite difference scheme [Eq. (20)] is only a first-order accurate algorithm with respect to the coordinate ξ. To construct a second-order scheme in ξ, the three-step implicit Richardson method is employed.

Step 1:

$$\left[\frac{1}{\Delta\xi/2}\left(\frac{\partial\tilde{\boldsymbol{E}}^*}{\partial\boldsymbol{U}}\right)^k_{i-\frac{1}{2}} + \frac{\partial}{\partial\eta}\left(\frac{\partial\tilde{\boldsymbol{F}}}{\partial\boldsymbol{U}}\right)^k_{i-\frac{1}{2}} - \frac{1-\omega_{i-\frac{1}{2}}-\omega_i}{\Delta\xi/2}\left(\frac{\partial\boldsymbol{P}^*}{\partial\boldsymbol{U}}\right)^k_{i-\frac{1}{2}}\right]\Delta^k\bar{\boldsymbol{U}}_{i-\frac{1}{2}}$$
$$= -\left\{\frac{\tilde{\boldsymbol{E}}^{*k}_{i-\frac{1}{2}} - \tilde{\boldsymbol{E}}^*_{i-1}}{\Delta\xi/2} + \left(\frac{\partial\tilde{\boldsymbol{F}}}{\partial\eta}\right)^k_{i-\frac{1}{2}} + \omega_{i-\frac{1}{2}}\frac{\boldsymbol{P}^{*k}_{i-\frac{1}{2}} - \boldsymbol{P}^{*k}_{i-1}}{\Delta\xi/2} + (1-\omega_i)\frac{\boldsymbol{P}^{*n-1}_i - \boldsymbol{P}^{*k}_{i-\frac{1}{2}}}{\Delta\xi/2}\right\}$$

$$\bar{\boldsymbol{U}}_{i-\frac{1}{2}} = \bar{\boldsymbol{U}}^k_{i-\frac{1}{2}} + \Delta^k\bar{\boldsymbol{U}}_{i-\frac{1}{2}} \tag{26}$$

Step 2:

$$\left[\frac{1}{\Delta\xi/2}\left(\frac{\partial\tilde{\boldsymbol{E}}^*}{\partial\boldsymbol{U}}\right)^k_i + \frac{\partial}{\partial\eta}\left(\frac{\partial\tilde{\boldsymbol{F}}}{\partial\boldsymbol{U}}\right)^k_i - \frac{1-\omega_i-\omega_{i+\frac{1}{2}}}{\Delta\xi/2}\left(\frac{\partial\boldsymbol{P}^*}{\partial\boldsymbol{U}}\right)^k_i\right]\Delta^k\bar{\boldsymbol{U}}_i$$
$$= -\left\{\frac{\tilde{\boldsymbol{E}}^{*k}_i - \tilde{\boldsymbol{E}}^*_{i-\frac{1}{2}}}{\Delta\xi/2} + \left(\frac{\partial\tilde{\boldsymbol{F}}}{\partial\eta}\right)^k_i + \omega_i\frac{\boldsymbol{P}^{*k}_i - \boldsymbol{P}^{*k}_{i-\frac{1}{2}}}{\Delta\xi/2} + \left(1-\omega_{i+\frac{1}{2}}\right)\frac{\boldsymbol{P}^{*n-1}_{i+\frac{1}{2}} - \boldsymbol{P}^{*k}_i}{\Delta\xi/2}\right\}$$

$$\bar{\boldsymbol{U}}_i = \bar{\boldsymbol{U}}^k_i + \Delta^k\bar{\boldsymbol{U}}_i \tag{27}$$

Step 3:

$$\left[\frac{1}{\Delta\xi}\left(\frac{\partial\tilde{\boldsymbol{E}}^*}{\partial\boldsymbol{U}}\right)^k_i + \frac{\partial}{\partial\eta}\left(\frac{\partial\tilde{\boldsymbol{F}}}{\partial\boldsymbol{U}}\right)^k_i - \frac{1-\omega_i-\omega_{i+1}}{\Delta\xi}\left(\frac{\partial\boldsymbol{P}^*}{\partial\boldsymbol{U}}\right)^k_i\right]\Delta^k\bar{\boldsymbol{U}}_i$$
$$= -\left\{\frac{\tilde{\boldsymbol{E}}^{*k}_i - \tilde{\boldsymbol{E}}^*_{i-1}}{\Delta\xi} + \left(\frac{\partial\tilde{\boldsymbol{F}}}{\partial\eta}\right)^k_i + \omega_i\frac{\boldsymbol{P}^{*k}_i - \boldsymbol{P}^{*k}_{i-1}}{\Delta\xi} + (1-\omega_{i+1})\frac{\boldsymbol{P}^{*n-1}_{i+1} - \boldsymbol{P}^{*k}_i}{\Delta\xi}\right\}$$

$$\bar{\boldsymbol{U}}_i = \bar{\boldsymbol{U}}_i{}^k + \Delta^k\bar{\boldsymbol{U}}_i \tag{28}$$

To get second-order accuracy with respect to ξ, the resulting solution at the marching station ξ_i is calculated as

$$\boldsymbol{U}_i = 2\bar{\boldsymbol{U}}_i - \bar{\boldsymbol{U}}_i \tag{29}$$

It can be shown that the first-order approximation of the streamwise pressure gradient component Eq. (24) combined with the three-step Richardson scheme results in a second-order-accurate algorithm for smooth flows.

In a manner similar to the scheme in Eq. (20), the derivatives $\partial/\partial\eta$ in Eqs. (26–28) are discretized by the second-order-accurate TVD scheme [Eqs. (21–25)].

Numerical results show that the Richardson scheme [Eqs. (26–29)] can be applied to capture strong shock waves and contact discontinuities with small numerical diffusion. One of the main advantages of the Richardson scheme is that the method is unconditionally stable. Therefore, it is possible to use large integration steps in the marching direction. The second-order upwind approximation and the good dispersive properties of the Richardson scheme enable one to resolve strong discontinuities with high accuracy and practically without nonphysical oscillations. In all test cases presented, shocks are smeared on one to two grid cells.

If the boundary conditions are treated explicitly, even though interior points are solved by implicit schemes, a Courant–Friedrichs–Lewy number of 1.0 will be the maximum possible for stability. To avoid this restriction, the boundary conditions (4–7) are approximated implicitly. The main difficulty that arises is associated with an implicit approximation of the boundary condition (7) imposed at a rigid surface. Inasmuch as it follows from the characteristic analysis of the Euler equations, the only boundary condition imposed at an impermeable wall is Eq. (7). To determine the other flow quantities, two types of impermeable wall conditions are implemented, depending on the freestream Mach number. For subsonic and transonic flow problems, the wall boundary conditions proposed in Ref. 20 are employed. An approach elaborated in Ref. 21 is applied to calculate boundary points for fully supersonic flows. These nonlinear boundary conditions can be represented in vector form as

$$\boldsymbol{B}(\boldsymbol{U}_0) + \boldsymbol{C}(\boldsymbol{U}_1) = 0 \tag{30}$$

By the application to the nonlinear equations (30) of the same Newton iterative method as for the difference scheme, one can write

$$\left(\frac{\partial \boldsymbol{B}}{\partial \boldsymbol{U}}\right)_0^k \Delta^k \boldsymbol{U}_0 + \left(\frac{\partial \boldsymbol{C}}{\partial \boldsymbol{U}}\right)_1^k \Delta^k \boldsymbol{U}_1 = -\left\{\boldsymbol{B}(\boldsymbol{U}_0^k) + \boldsymbol{C}(\boldsymbol{U}_1^k)\right\} \quad (31)$$

The linear system of equations (31) is naturally incorporated into the numerical algorithm [Eqs. (26–28)], and the factorization error is reduced to zero at the boundary points as well as in the interior of the computational domain.

V. Parabolic Pressure-Correction Procedure

For essentially subsonic flows, the convergence rate of the method of global iterations is slow because in subsonic regions the pressure correction due to the use of forward differences can propagate only one station upstream per iteration. Thus, as many iterations as there are grid points in the marching direction should be executed until the downstream boundary condition influence reaches the inlet. Because the information about the solution is transmitted from the previous iteration to the current global iteration by the pressure field only, the convergence of the iteration process can be accelerated by an appropriate pressure-correction procedure.

To derive a parabolic pressure-correction equation that takes into account the characteristic properties of the Euler equations, an auxiliary Poisson equation for the pressure field is employed. Differentiating the ξ-momentum equation with respect to ξ and the η-momentum equation multiplied by an arbitrary constant μ with respect to η and summing both equations, we obtain the following Poisson equation:

$$\begin{aligned} &y_\eta p_{\xi\xi} + \mu x_\xi p_{\eta\eta} - (x_\eta + \mu y_\xi) p_{\xi\eta} \\ &\quad + (\mu - 1)[x_{\xi\eta} p_\eta - y_{\xi\eta} p_\xi] = y_\eta (p_\xi)_\xi + \mu x_\xi (p_\eta)_\eta \\ &\quad - (x_\eta + \mu y_\xi)(p_\xi)_\eta + (\mu - 1)[x_{\xi\eta}(p_\eta) - y_{\xi\eta}(p_\xi)] \end{aligned} \quad (32)$$

The constant μ plays the role of a diffusion factor. The components of the pressure gradient on the right-hand side of Eq. (32) are calculated from the momentum equations of the Euler system of equations.

Because the velocity components, total energy, density, and pressure are computed using the coupled algorithm [Eq. (20)], there is no need to use the separate pressure Poisson equation to satisfy the continuity equation as is done in Ref. 12. In the present method, the continuity, momentum, and energy equations are satisfied automatically at each marching station. It should be emphasized that Eq. (32) is required only to construct the parabolic pressure-correction equation needed to accelerate the convergence of the pressure-relaxation procedure.

Let us consider three different pressure fields: 1) the pressure distribution $\tilde{p}$ calculated from the current marching sweep, 2) the pressure field p^{n-1} found from the previous global iteration, and 3) the corrected pressure field p^n required for the next global iteration. The pressure correction equation can be derived by calculating the left-hand side of Eq. (32) using the corrected pressure values, whereas the right-hand side is treated as a source term and is approximated by the finite difference scheme (20–25). To simplify the Poisson equation written earlier, we assume that the corrected values of the first and mixed derivatives in Eq. (32) are equal to the similar terms on the right-hand side and can, therefore, be canceled, yielding

$$y_\eta p^n_{\xi\xi} + \mu x_\xi p^n_{\eta\eta} = y_\eta (\tilde{p}_\xi)_\xi + \mu x_\xi (\tilde{p}_\eta)_\eta \quad (33)$$

By taking into account the streamwise pressure gradient splitting Eq. (8), one can rewrite Eq. (33) as follows:

$$\begin{aligned} &y_\eta \left[\frac{\partial}{\partial \xi}\left(\omega \frac{\partial p^n}{\partial \xi}\right) + \frac{\partial}{\partial \xi}\left((1-\omega)\frac{\partial p^n}{\partial \xi}\right)\right] + \mu x_\xi \frac{\partial^2 p^n}{\partial \eta^2} \\ &\quad = y_\eta \left[\frac{\partial}{\partial \xi}\left(\omega \frac{\partial \tilde{p}}{\partial \xi}\right) + \frac{\partial}{\partial \xi}\left((1-\omega)\frac{\partial p^{n-1}}{\partial \xi}\right)\right] + \mu x_\xi \frac{\partial^2 \tilde{p}}{\partial \eta^2} \end{aligned} \quad (34)$$

Because the first term in Eq. (34) is incorporated implicitly into the streamwise marching process, this term can be treated as the corrected pressure gradient value and set equal to the analogous term on the right-hand side, so that Eq. (34) is reduced to give

$$\begin{aligned} &y_\eta \frac{\partial}{\partial \xi}\left((1-\omega)\frac{\partial p^n}{\partial \xi}\right) + \mu x_\xi \frac{\partial^2 p^n}{\partial \eta^2} \\ &\quad = y_\eta \frac{\partial}{\partial \xi}\left((1-\omega)\frac{\partial p^{n-1}}{\partial \xi}\right) + \mu x_\xi \frac{\partial^2 \tilde{p}}{\partial \eta^2} \end{aligned} \quad (35)$$

Approximating the left-hand side with central differences and using the same approximation for the the right-hand side as in the difference scheme, we can write Eq. (35) in difference form:

$$\begin{aligned} &(y_\eta)_{i,j}(1-\omega_i)\frac{p^n_{i-1,j} - 2p^n_{i,j} + p^n_{i+1,j}}{\Delta \xi^2} \\ &\quad + \mu (x_\xi)_{i,j} \frac{p^n_{i,j-1} - 2p^n_{i,j} + p^n_{i,j+1}}{\Delta \eta^2} \\ &\quad = (y_\eta)_{i,j}(1-\omega_i)\frac{\tilde{p}_{i-1,j} - p^{n-1}_{i,j} - \tilde{p}_{i,j} + p^{n-1}_{i+1,j}}{\Delta \xi^2} \\ &\quad + \mu (x_\xi)_{i,j} \frac{\tilde{p}_{i,j-1} - 2\tilde{p}_{i,j} + \tilde{p}_{i,j+1}}{\Delta \eta^2} \end{aligned} \quad (36)$$

Equation (36) has been obtained assuming that ω only weakly depends on ξ.

To avoid the solution of the elliptic equation, we parabolize Eq. (36) so that the streamwise pressure gradient term at point $(i-1, j)$ is assumed to be equal to the corrected pressure gradient term evaluated at the same point:

$$p^n_{i,j} - p^n_{i-1,j} \cong p^{n-1}_{i,j} - \tilde{p}_{i-1,j} \quad (37)$$

Substituting Eq. (37) into Eq. (36) and defining pressure corrections as

$$\epsilon_{i,j} = \tilde{p}_{i,j} - p^{n-1}_{i,j}, \qquad \delta_{i,j} = p^n_{i,j} - p^{n-1}_{i,j} \quad (38)$$

we derive the following finite difference equation:

$$\begin{aligned} &\mu_1 \delta_{i,j-1} - [2\mu_1 + (1-\omega_i)]\delta_{i,j} + \mu_1 \delta_{i,j+1} \\ &\quad = \mu_1 \epsilon_{i,j-1} - [2\mu_1 + (1-\omega_i)]\epsilon_{i,j} + \mu_1 \epsilon_{i,j+1} - (1-\omega_i)\delta_{i+1,j} \end{aligned} \quad (39)$$

with $\mu_1 = (x_\xi / y_\eta)_i (\Delta \xi^2 / \Delta \eta^2)\mu$. Equation (39) is a parabolic pressure-correction equation for δ.

The numerical solution procedure can be represented as a predictor-corrector scheme. In the predictor step, the modified Euler equations (18) are solved using the space-marching method based on the streamwise pressure gradient splitting Eq. (8). This generates $\tilde{p}$ that, together with the pressure p^{n-1} obtained from the previous global iteration, is used in the corrector step (39) to find the corrected pressure field p^n.

As a result of the solution of (39), the pressure correction caused by the downstream boundary condition $\delta_{I,j} = \epsilon_{I,j}$ is rapidly propagated from the outflow to the inflow boundary. If an excessive skewing of the transverse pressure profiles is caused by the correction equation (39) the diffusion factor μ should be increased. It allows one to control the degree to which the transverse pressure profiles are preserved. In the present calculations the diffusion factor μ was varied from 50 to 80.

In contrast to the approach developed in Ref. 4 for incompressible flows, the present pressure-correction procedure can be employed for the compressible form of the Euler equations at all speeds. Indeed, in regions where the flow is subsonic and, consequently, according to Eq. (10), $\omega < 1$, the parabolic pressure-correction procedure transmits information in the upstream direction that corresponds to the elliptic nature of Eq. (3). At the same time, for supersonic flowfields, $\omega = 1$, and Eq. (39) can be solved analytically, yielding

$$\delta_{i,j} = \epsilon_{i,j} \quad (40)$$

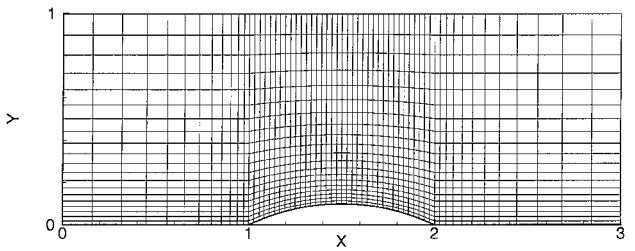

Fig. 1 Computational 61 × 21 grid.

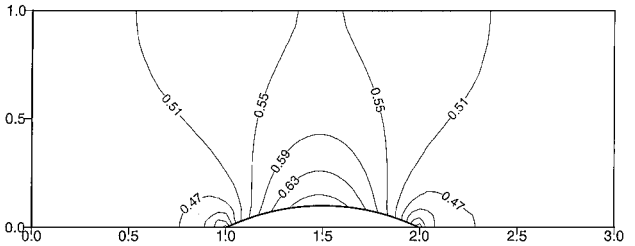

Fig. 2 Iso-Mach lines for subsonic flow $M_{-\infty} = 0.5$ in the duct with 10% circular arc bump.

Equation (40) means that no corrections are made in supersonic flow regions.

Consequently, the parabolic pressure-correction procedure (39) can be applied for both subsonic and supersonic flowfields and is consistent with the characteristic properties of the governing equations. It should be emphasized that the computing time required to solve the parabolic equations (39) is much less than the computational effort needed for executing one space-marching sweep.

Numerical calculations show that underrelaxation of the predicted pressure correction is necessary; therefore, the resulting pressure field is calculated by

$$p^n_{i,j} = p^{n-1}_{i,j} + \tau \delta_{i,j} \tag{41}$$

where τ is a relaxation parameter ($0 < \tau \leq 1$), which was chosen 0.5 for subsonic and transonic calculations presented.

VI. Results and Discussion

To validate the present iterative space-marching method for calculating inviscid flows ranging from fully subsonic to transonic and fully supersonic, the flow in a channel with a circular arc bump has been chosen as a test problem. This problem has been studied and, therefore, is well suited for code testing. Two circular arc bump thickness-to-chord ratios were used: 10% for subsonic and transonic simulations and 4% for supersonic flow calculation. The duct width is equal to the bump chord length, and the channel length is equal to three bump chords. A typical 61 × 21 nonuniform grid used for subsonic and transonic calculations is shown in Fig. 1. The grid points are stretched in the bump region and near the lower wall. For supersonic calculations, a uniform grid in both spatial directions is employed. In the subsonic and transonic cases, the nonuniform grids are symmetrical with respect to the bump midchord, whereas for the supersonic flow problem, half of the physical domain in front of the bump is cut off and not calculated because the flow is uniform in this region. For all test calculations, the flow in the channel is initially uniform with the far upstream flow properties. The outflow static pressure is imposed so that the static-to-stagnation pressure ratio corresponds to the far upstream Mach number in one-dimensional steady isentropic flow. The solution is assumed to have reached steady-state when the maximum pressure residual

$$\max_{i,j} \left| 1 - p^{n-1}_{i,j} / p^n_{i,j} \right| / \tau$$

is less than a prescribed error level, which was set to 10^{-4} in our calculations.

A. Subsonic Flow Test

In the first test problem, the subsonic inviscid flow with an upstream Mach number $M_{-\infty} = 0.5$ in a channel with a 10% circular arc bump on the lower wall is calculated. Figure 2 shows iso-Mach lines of the steady-state solution calculated on a 51 × 16 grid using the proposed method of global iterations together with the parabolic pressure-correction procedure. A little asymmetry is seen on the lower wall, which is apparently caused by the numerical implementation of the wall boundary condition (6) at the singular points. To estimate the effect of grid spacing on the numerical solution, the Mach number distributions along the lower and upper walls obtained on 31 × 11, 51 × 16, and 81 × 31 grids are compared with the calculations of Eidelman et al.[22] in Fig. 3. As one can see, all of the computed surface Mach number distributions are in good agreement with the numerical results of Ref. 22. Note that the second-order

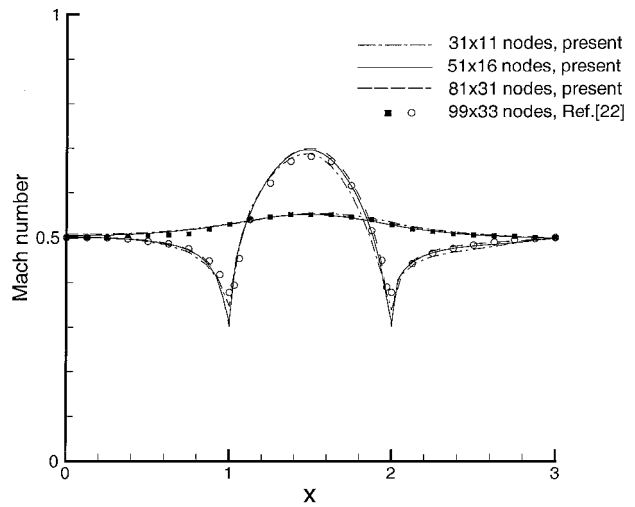

Fig. 3 Surface Mach number distribution for subsonic flow $M_{-\infty} = 0.5$ in the duct with 10% circular arc bump.

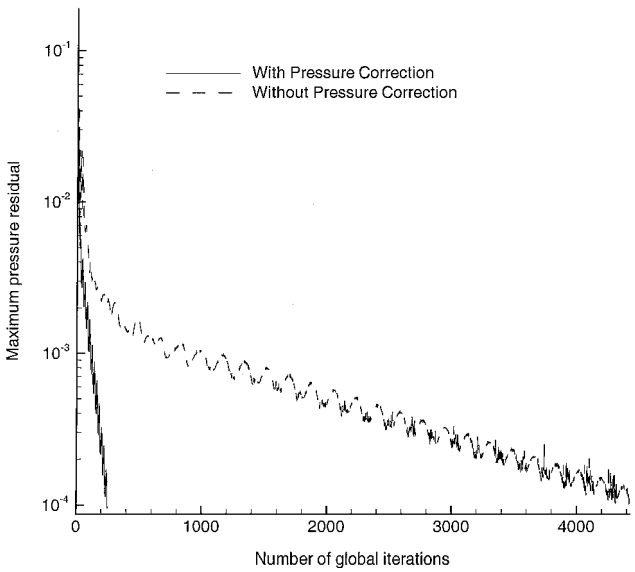

Fig. 4 Convergence history for subsonic flow $M_{-\infty} = 0.5$ in the duct with 10% circular arc bump.

Richardson scheme has very good dissipation properties resulting in a better resolution of the local extrema of the solution than the second-order upwind TVD scheme used in Ref. 22. The main reason for that behavior is that, in contrast to the Richardson approximation, the TVD scheme is only a first-order method in the vicinity of local extrema of the solution. For the 51 × 16 grid, the convergence histories obtained using the basic iterative space-marching method without the pressure-correction and alternatively with the parabolic pressure-correction procedure are compared in Fig. 4. The convergence acceleration factor due to the pressure correction procedure is about 20 for this test problem.

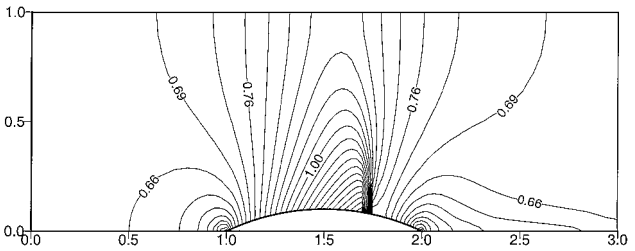

Fig. 5 Iso-Mach lines for transonic flow $M_{-\infty} = 0.675$ in the duct with 10% circular arc bump.

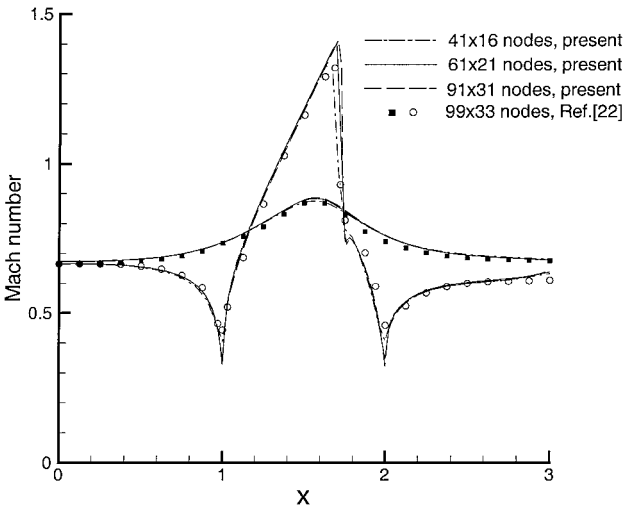

Fig. 6 Surface Mach number distribution for transonic flow $M_{-\infty} = 0.675$ in the duct with 10% circular arc bump.

B. Transonic Flow Test

In the second test calculation, the same duct geometry as for the preceding problem is considered, but the upstream Mach number was chosen as $M_{-\infty} = 0.675$. Figures 5 and 6 present iso-Mach contours and the wall Mach number distribution, respectively. The upstream Mach number is sufficiently high to produce a local supersonic region on the bump. The supersonic region is terminated by a shock located at 73% of the bump chord, as shown in Fig. 5. One can see in Fig. 6 that the grid refinement leads to sharper profiles of the solution at the shock and at the leading and trailing edges of the bump, whereas in the smooth part of the solution, the results are practically unchanged and in good agreement with calculations presented in Ref. 22. For all of the grids used, the shock is smeared only over two grid cells. As in the preceding test example, the application of the Richardson scheme results in better resolution of the local extrema of the solution compared to the numerical results of Ref. 22. To demonstrate the convergence acceleration due to the pressure-correction procedure, two histories of convergence obtained on the 61×21 grid are shown in Fig. 7. To reach the steady-state solution, about 430 global iterations were required using the basic method of global iterations, whereas less than half of this number was needed when the pressure-correction procedure was applied after each marching sweep.

C. Supersonic Flow Test

The last test problem is the supersonic inviscid flow with the upstream Mach number $M_{-\infty} = 1.65$ in a channel with a 4% circular arc bump. Because the flow is supersonic in the whole physical domain, two oblique shocks are generated at both ends of the bump. The leading-edge shock is reflected from the upper duct wall and then interacts with an expansion fan generated by the circular arc bump. Then the reflected shock wave interacts with the trailing-edge shock. After the interaction, both shock waves leave the computational domain. To demonstrate the ability of the present method to resolve shocks, rarefaction waves and their interaction iso-Mach contours calculated on a 61×31 grid are presented in Fig. 8. As with the preceding test problems, the grid convergence analysis has

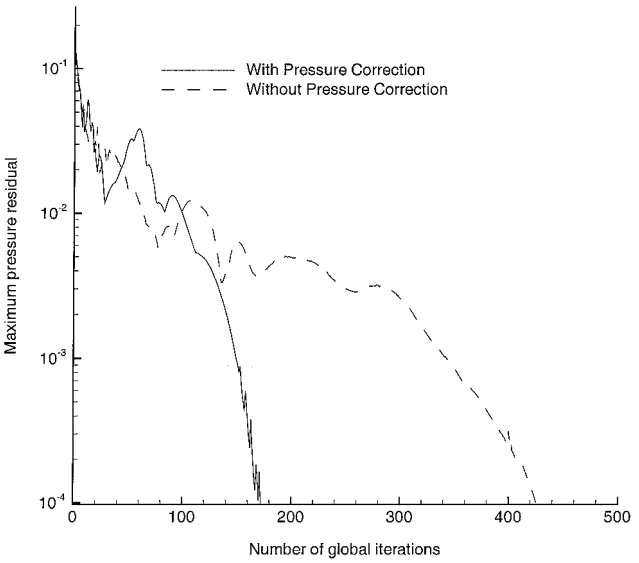

Fig. 7 Convergence history for transonic flow $M_{-\infty} = 0.675$ in the duct with 10% circular arc bump.

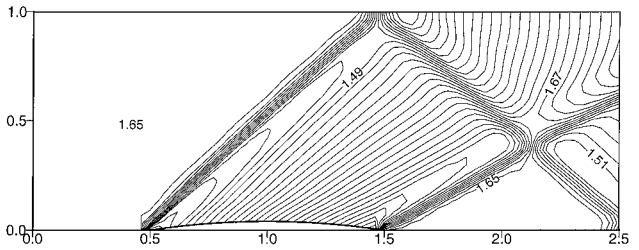

Fig. 8 Iso-Mach lines for transonic flow $M_{-\infty} = 1.65$ in the duct with 4% circular arc bump.

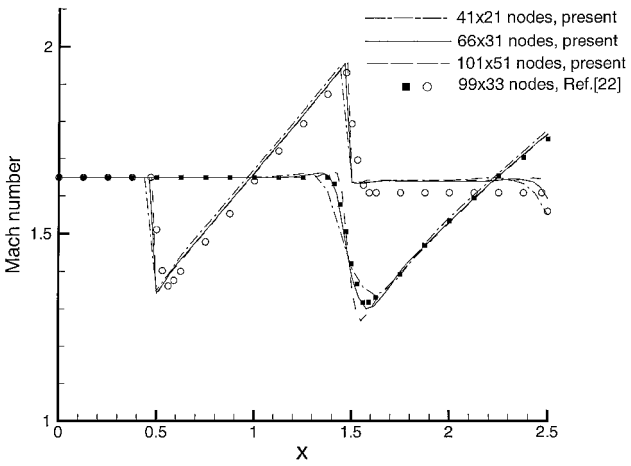

Fig. 9 Surface Mach number distribution for transonic flow $M_{-\infty} = 1.65$ in the duct with 4% circular arc bump.

been performed. Figure 9 shows the comparison of the wall Mach number distributions computed on 41×21, 66×31, and 101×51 grids with the numerical results of Ref. 22. The agreement is very good; however, the present scheme captures the shocks at the leading and trailing edges of the bump within one grid cell, whereas the second-order upwind TVD scheme[22] results in the smearing of the shocks over three grid cells. Note that as the shocks propagate across the channel the numerical dissipation smears the discontinuities over two grid cells. For this test problem, the present iterative space-marching method simplifies to a single marching sweep. That happens because the flow is fully supersonic, and as follows from Eqs. (8–10), the streamwise pressure gradient component can be calculated implicitly in the entire computational domain, that is, $\omega = 1.0$ in Eqs. (17) and (18).

The typical computational time required for solving the first test problem, which was the most time consuming, was about 15 min on a Hewlett–Packard 9000/780/160 work station if the parabolic pressure-correction procedure was employed.

VII. Conclusions

A new method of global iterations based on the fully coupled iterative space-marching technique and the parabolic pressure-correction procedure has been developed to solve the Euler equations for compressible fluid flows. The main advantage of this approach is that the same method can be applied to calculate compressible subsonic, transonic, and supersonic flows. The global iterations are carried out with respect to the streamwise pressure gradient component, which is evaluated by backward differences in supersonic regions and by forward differences in subsonic flowfields. This approximation is consistent with hyperbolic–elliptic properties of the Euler equations for compressible flows and permits a stable space-marching sweep to be executed at all Mach numbers. Multiple sweeps are required to resolve the elliptic effects of subsonic and transonic flows. A new fully coupled iterative scheme based on a Newton approach is developed to solve the nonlinear system of equations resulted from the discretization procedure. There are two main advantages of the present technique, namely, the system of nonlinear equations is solved in a fully coupled manner and the factorization error is vanished on convergence. An implicit second-order Richardson scheme and a second-order symmetric TVD scheme are used to approximate the streamwise and transverse derivatives, respectively. The present technique allows to resolve strong shock waves, rarefaction fans, and their interaction with small numerical dissipation and without spurious oscillations. The new parabolic pressure-correction procedure, taking into account the characteristic nature of the Euler equations, has been implemented to accelerate the convergence rate of the method of global iterations. Numerical results show that the method presented is accurate, is robust, and can efficiently be applied to solve the Euler equations for sub-, trans-, and supersonic flows.

Although only the Euler equations are considered in the present analysis, extension to the parabolized Navier–Stokes (PNS) equations is quite straightforward if there is no streamwise separation in the flowfield. Actually, as it has been shown by Vigneron et al.,[7] that the same streamwise pressure gradient splitting [Eq. (8 and 9)] can be used to make the modified PNS equations parabolic in the entire computational domain. In other words, the iterative space-marching method described in Sec. III is applicable for solving the PNS equations for sub-, trans-, and supersonic flows if no streamwise separation occurs. The main difficulties associated with the application of the present iterative space-marching method to viscous flows is flow separation. To overcome this obstacle, a new streamwise flux vector splitting has been developed. The new splitting takes into account the elliptic properties of the streamwise convective terms that make the space-marching procedure stable in regions of flow recirculation. This method will be the subject of a forthcoming paper.

Acknowledgment

This work was supported by the Alexander von Humboldt Foundation (Germany) under Grant IV.4-RUS 1039319 STP.

References

[1]Rubin, S. G., and Reddy, D. R., "Analysis of Global Pressure Relaxation for Flows with Strong Interaction and Separation," *Computers and Fluids*, Vol. 11, No. 4, 1983, pp. 281–306.

[2]Israeli, M., and Lin, A., "Iterative Numerical Solutions and Boundary Conditions for the Parabolized Navier–Stokes Equations," *Computers and Fluids*, Vol. 13, No. 4, 1985, pp. 397–409.

[3]Liu, X., and Pletcher, R. H., "A Coupled Marching Procedure for the Partially Parabolized Navier–Stokes Equations," *Numerical Heat Transfer*, Vol. 10, 1986, pp. 539–556.

[4]TenPas, P. W., and Pletcher, R. H., "Coupled Space-Marching Method for the Navier–Stokes Equations for Subsonic Flows," *AIAA Journal*, Vol. 29, No. 2, 1991, pp. 219–226.

[5]Davis, R. T., "Numerical Solution of the Hypersonic Viscous Shock Layer Equations," *AIAA Journal*, Vol. 8, No. 5, 1970, pp. 843–851.

[6]Lubard, S. C., and Helliwell, W. S., "Calculation of the Flow on a Cone at High Angle of Attack," *AIAA Journal*, Vol. 12, 1974, pp. 965–974.

[7]Vigneron, Y. C., Rakich, J. V., and Tannehill, J. C., "Calculation of Supersonic Viscous Flow over Delta Wings with Sharp Subsonic Leading Edges," AIAA Paper 78-1173, 1978.

[8]Newsome, R. W., Walters, R. W., and Thomas, J. L., "An Efficient Iteration Strategy for Upwind/Relaxation Solutions to the Thin-Layer Navier–Stokes Equations," AIAA Paper 87-1113, 1987.

[9]Schiff, L. B., and Steger, J. L., "Numerical Simulation of Steady Supersonic Viscous Flow," AIAA Paper 79-0130, 1979.

[10]Lin, A., and Rubin, S. G., "Three-Dimensional Supersonic Viscous Flow over a Cone at Incidence," *AIAA Journal*, Vol. 20, No. 11, 1982, pp. 1500–1507.

[11]Tirskii, G. A., Utyuzhnikov, S. V., and Yamaleev, N. K., "Efficient Numerical Method for Simulation of Supersonic Viscous Flow Past a Blunted Body at a Small Angle of Attack," *Computers and Fluids*, Vol. 23, No. 1, 1994, pp. 103–114.

[12]Patankar, S. V., and Spalding, D. B., "A Calculation Procedure for Heat, Mass and Momentum Transfer in Three Dimensional Parabolic Flows," *Numerical Heat Transfer*, Vol. 15, 1972, pp. 1787–1806.

[13]Karki, K., and Patankar, S. V., "Pressure-Based Calculation Procedure for Viscous Flows at All Speeds in Arbitrary Configurations," *AIAA Journal*, Vol. 27, No. 9, 1989, pp. 1167–1174.

[14]Kobayashi, M. H., and Pereira, J. C. F., "Characteristic-Based Pressure Correction at All Speeds," *AIAA Journal*, Vol. 34, No. 2, 1996, pp. 272–280.

[15]Rincon, J., and Elder, R., "A High-Resolution Pressure-Based Method for Compressible Flows," *Computers and Fluids*, Vol. 26, No. 3, 1997, pp. 217–231.

[16]Davis, R. T., Barnett, M., and Rakich, J. V., "The Calculation of Supersonic Viscous Flows Using the Parabolized Navier–Stokes Equations," *Computers and Fluids*, Vol. 14, No. 3, 1986, pp. 197–224.

[17]Khosla, P. K., and Lai, H. T., "Global Relaxation Procedure for Compressible Solutions of the Steady-State Euler Equations," *Computers and Fluids*, Vol. 15, No. 2, 1987, pp. 215–229.

[18]Beam, R., and Warming, R. F., "An Implicit Factored Scheme for the Compressible Navier–Stokes Equations," *AIAA Journal*, Vol. 16, 1978, pp. 393–401.

[19]Yee, H. C., "Construction of Explicit and Implicit Symmetric TVD Schemes and Their Applications," *Journal of Computational Physics*, Vol. 68, 1987, pp. 151–179.

[20]Thompkins, W. T., "Solution Procedures for Accurate Numerical Simulations of Flow in Turbomachinery Cascades," AIAA Paper 83-0257, 1983.

[21]Marsilio, R., "Vortical Solutions in Supersonic Corner Flows," *AIAA Journal*, Vol. 31, No. 9, 1993, pp. 1651–1658.

[22]Eidelman, S., Colella, P., and Shreeve, R. P., "Application of the Godunov Method and Its Second-Order Extension to Cascade Flow Modeling," *AIAA Journal*, Vol. 22, No. 11, 1984, pp. 1609–1615.

S. K. Aggarwal
Associate Editor